Brief Communication

Elementary Properties of Axonal Calcium Currents in Type B Photoreceptors in *Hermissenda crassicornis*

Catherine T. Tamse[1] **and Ebenezer N. Yamoah**[1,2]

[1]*Center for Neuroscience, Department of Otolaryngology, University of California, Davis, Davis, California 95616, and* [2]*Marine Biological Laboratory, Woods Hole, Massachusetts 02543*

Axons of the type B photoreceptors form synapses with hair cells and interneurons that are involved in classical conditioning in *Hermissenda*. We examined the differences in the Ca^{2+} channels expressed in the soma and axons of the B photoreceptors by direct functional recordings of single-channel currents. Although the soma of the B cells express two Ca^{2+} current subtypes, a transient BayK 8644-insensitive (~17 pS) current and a sustained BayK 8644-sensitive (~10 pS) current, the axons expressed only the latter. The axonal Ca^{2+} current activated at potentials positive to −20 mV. Moreover, the Ca^{2+} channels are distributed heterogeneously along the length of the axon, with the higher channel density (~10–15 channel μm^{-2}) occurring at the distal one-third of the isolated axons, with respect to the soma. The regions of Ca^{2+} channel clusters may represent the presynaptic site of the photoreceptor–interneuron synapses. Furthermore, the high-density clusters of Ca^{2+} channels may augment postsynaptic responses. The results of the present study represent the first direct recordings of Ca^{2+} currents at presumed synaptic sites. Expression of different Ca^{2+} channel subtypes at distinct compartments of the type B photoreceptors may generate diverse Ca^{2+} domains that may be required for neuronal plasticity in *Hermissenda*.

Key words: learning; memory; calcium currents; presynaptic calcium channels; photoreceptors; neuronal plasticity; Hermissenda

Classical conditioning in the invertebrate mollusk, *Hermissenda crassicornis*, after repeated exposures to paired light and motion entails cellular changes in the sensory interactions between the vestibular hair cells, the ocular photoreceptors (Crow and Alkon, 1980; Alkon et al., 1985, 1998; Crow, 1985), and interneurons (Hodgson and Crow, 1992). Studies have shown that type B photoreceptors undergo memory-associated changes, which are generated through enhanced membrane excitability linked to increased input resistance (Alkon et al., 1982; Tomsic and Alkon, 2000) and a reduction in several K^+ conductances (Alkon et al., 1985). The enhanced synaptic facilitation after conditioning (Schuman and Clark, 1994; Frysztak and Crow, 1997), the differential membrane properties (Yamoah and Crow, 1996; Yamoah et al., 1998) between type B and type A photoreceptors, as well as the synaptic organization of identified photoreceptors and other visual pathway neurons have also been investigated (Crow and Tian, 2000, 2002). However, the aforementioned learning-induced changes have all been analyzed at the soma membrane, whereas little or no information has been reported at the axonal site where the synaptic connections between hair cells, interneurons, and photoreceptors occur.

A fundamental characteristic of learning and memory involves not only changes in the membrane properties but increased efficacy of neurons at the synaptic level, such as in long-term potentiation (LTP) (Lynch et al., 1990; Staubli and Rogers, 1994; Malenka and Nicoll, 1999). Moreover, the enhanced synaptic strength as initiated by Ca^{2+} influx (Lynch et al., 1990) and the consequent rise in intracellular Ca^{2+} of presynaptic cells seem to be the crucial key to LTP (Linden and Ahn, 1999; Malenka and Nicoll, 1999).

The cellular modifications observed in conditioned *Hermissenda* have only been observed at the soma of photoreceptors, but changes at the synaptic sites between hair cells, interneurons, and photoreceptors still remain uncertain. Because Ca^{2+} influx is critical for neurotransmitter release at the synapses, and Ca^{2+} initiates several short- and long-term changes in neurons, we determined what unique properties axonal Ca^{2+} channels of the photoreceptors would contribute to the steps in the mechanisms of plasticity in *Hermissenda*.

MATERIALS AND METHODS

Isolation of soma and axons of type B photoreceptors. H. crassicornis were purchased from Sea Life Supply (Sand City, CA). Animals were held in modified 50 ml tubes, housed in an artificial seawater (ASW) tank, and maintained at 12–14°C. *Hermissenda* were fed scallops and kept on a 12 hr light/dark cycle. Details of the procedure for isolation of the eyes and photoreceptors of *Hermissenda* have been described previously by Yamoah and Crow (1994). The CNS was dissected in ASW and allowed to stand for 10 min at 4°C. These were then treated with an enzyme mixture consisting of protease XXIV (1 mg/ml) (Sigma, St. Louis, MO) and dispase II (5 mg/ml ASW) (Boehringer Mannheim, Mannheim, Germany) in ASW. The CNS was digested for 15–20 min at 4°C and for another 10–20 min at room temperature. The preparation was washed using ASW at 4°C. The eyes were removed surgically, desheathed, transferred into a recording chamber (35 mm sterile culture dish), and observed with an Olympus inverted microscope (IX70; Olympus Optical, Tokyo, Japan). Photoreceptors were identified as type A or B on the basis of their position relative to the lens and optic nerve (see Fig. 1*A,B*) (Yamoah and Crow, 1996). Isolated eyes without a lens and the stump of the optic nerve were therefore discarded. For experiments that required the type B photoreceptor axons, only preparations with an axon length of ≥90 μm were considered acceptable. Using the soma as the reference,

Received Aug. 29, 2002; revised Oct. 2, 2002; accepted Oct. 9, 2002.

This work was supported by National Science Foundation Grant IBN0196080 (E.N.Y.).

Correspondence should be addressed to Ebenezer N. Yamoah, Center for Neuroscience, Department of Otolaryngology, University of California, Davis, 1544 Newton Court, Davis, CA 95616. E-mail: enyamoah@ucdavis.edu.

isolated axons were divided arbitrarily into three equal parts: proximal one-third, middle third, and distal one-third. The average yield for axon isolation procedure was one photoreceptor per animal.

Chemicals and solutions. All chemicals were obtained from Sigma, unless indicated otherwise. ASW was composed of the following (in mM): 390 NaCl, 10 KCl, 10 $CaCl_2$, 23 $MgCl_2$, 25 $MgSO_4$, 15 HEPES, and 10 D-glucose. The solution was sterile filtered, and the pH was adjusted to 7.8 with 1 M NaOH. Whole-cell Ca^{2+} currents were recorded using external solution consisting of (in mM): 300 choline chloride, 50 $MgCl_2$, 20 $CaCl_2$, 10 glucose, 5 4-aminopyridine (4-AP), 100 tetraethylammonium acetate (TEA-acetate), and 15 HEPES, sterile filtered and adjusted to a pH of 7.7 with 1 M TEA-OH. The pipette or internal solution was made up of the following (in mM): 300 CsCl, 300 *N*-methyl-D-glucamine, 10 glutathione (reduced), 5 EGTA, 20 TEA-Cl, 5 Mg(ATP), 1 Na_2(GTP), and 40–50 HEPES, pH 7.4, with TEA-OH. Stock solution of 100 mM BayK 8644 (Calbiochem, La Jolla, CA) was made with DMSO and stored at −20°C. Aliquots of the stock solution were added to bath solutions to obtain the desired concentration (10 μM). For single-channel recordings, the bath solution contained (in mM): 350 K-glutamate, 100 TEA-Cl, 50 $MgCl_2$, 10 D-glucose, 10 $CaCl_2$, 5 4-AP, and 10 HEPES, and was adjusted to a pH of 7.4 with TEA-OH to shift the resting potential to ~0 mV. Patch electrodes were filled with (in mM): 250 Ba^{2+}, 100 TEA-Cl, 5 4-AP, and 10 HEPES, pH adjusted to 7.4 with TEA-OH. Osmolarity of all solutions ranged from 0.96 to 1 Osm.

Whole-cell and single-channel Ca^{2+}/Ba^{2+} current recordings and analysis. Whole-cell recordings were performed using standard patch-clamp recordings with the Axopatch 200B amplifier (Axon Instruments, Foster City, CA) (Hamill et al., 1981). Patch pipettes [borosilicate glass capillaries; 1.5 mm outer diameter (OD) and 1 mm inner diameter (ID)] (World Precision Instruments, Sarasota, FL) were pulled with a horizontal electrode puller (Model P-97; Sutter Instruments, Novato, CA). The tips of the pipette were fire polished using a micro-forge (MF-830; Narishige, Tokyo, Japan) to obtain tip diameters of ~1 μm. The pipette resistances were 1.2 ± 0.6 MΩ (n = 30) using the pipette solution described above. A 3% agar bridge with 1 M KCl was used as a reference electrode. For single-channel recordings, the cell-attached configuration was used. Patch pipettes were made from borosilicate glass with 2 mm OD and 1 mm ID. The tips of the electrodes were fire polished, and regions close to the tips (~10 μm) were coated with Sylgard (Dow Corning, Midland, MI) to reduce the capacitance of the electrodes. Patch pipettes filled with single-channel recording solution had resistances of 1.1 ± 0.7 MΩ (n = 51). Single-channel patches with seal resistances of >5 GΩ were considered to be acceptable for analysis. Single-channel currents were filtered at 1–2 kHz using a low-pass Bessel filter, sampled at 10–40 kHz, and stored in a personal computer. The channels were activated at a frequency of 0.2 Hz. Currents were digitized through an analog-to-digital converter (Digidata 1200; Axon Instruments). Data collection of the whole-cell current was controlled with pClamp software (version 8.0; Axon Instruments). However, single-channel currents were acquired using a custom-written software. Data analysis of recorded whole-cell Ca^{2+} currents was performed using Clampfit 8.1 (Axon Instruments) and Origin 6.0 (Microcal Software, Northampton, MA).

Analysis of single-channel currents was performed using a custom-written software, which is linked to Origin software (Microcal). Leak and capacitative currents were corrected off-line by fitting smooth templates to null traces and subtracting them from active traces. Open–close transitions were detected using half-height threshold analysis criteria. Idealized records were used to generate amplitude histograms and then fitted to a single Gaussian distribution using a Levenberg–Marquardt algorithm to obtain the mean single-channel amplitude and SD. We used a minimum of five voltage steps and their corresponding single-channel currents to determine the unitary conductance. The single-channel current–voltage relationship was fitted by a linear least-square regression line, and single-channel conductance was obtained from the slope of the regression line. Idealized records were also used to construct ensemble-averaged currents and open probability as well as closed- and open-time histograms. All experiments were performed at room temperature (~21°C). Where appropriate, pooled data were presented as means ± SD.

RESULTS

We have shown previously that at least two Ca^{2+} current subtypes (sustained and transient current) are expressed in the soma of the type B photoreceptors (Yamoah and Crow, 1994). Shown in Figure 1*C* are Ca^{2+} current traces recorded from a type B photoreceptor, from a holding potential of −80 mV to a test potential of 10 mV. When the same cell was held at −30 mV and stepped to the same test potential, the transient component was suppressed, and the sustained current became apparent. We have reported that the sustained current is sensitive to the dihydropyridines, but the transient current is not (Yamoah and Crow, 1994). To further identify the channels, single-channel currents were recorded using cell-attached patches from type B photoreceptors. Figure 1*D* illustrates a family of single-channel Ba^{2+} currents that were recorded before and after the application of 10 μM BayK 8644. Aside from its sensitivity toward BayK 8644, the current was activated from a holding potential of −30 mV and remained open at the end of a ~300 msec test pulse. This single-channel current thus represents the sustained component. The increase in long openings after application of the dihydropyridine agonist BayK 8644 is a characteristic feature of L-type Ca^{2+} channels in vertebrate neurons and cardiac cells (Fox et al., 1987; Rodriguez-Contreras and Yamoah, 2001). Moreover, the concentrations of the drug used in these experiments were slightly higher than that required for vertebrate cells. The higher concentrations may be necessary for the high ionic strength of the seawater solutions used for the recordings (Yamoah et al., 1994).

To record the single-channel currents of the transient component, nitrendipine (20 μM) was included in the patch pipettes to block the sustained current. Similar methods have been used to isolate single L-type channels in vertebrate hair cells (Rodriguez-Contreras and Yamoah, 2001). The ensuing single-channel current had frequent openings at the first 100 msec of the test potentials and was apparent when patches were held at a more negative holding potential (less than −70 mV) (Fig. 1*E*). Shown in Figure 1*F* are the single-channel current–voltage relationships of the two subtypes of Ba^{2+} currents in the B photoreceptors. The slope conductances of the regression lines for the BayK 8644-sensitive and -insensitive currents were 10 and 17 pS, respectively. Patch pipettes containing either 500 μM Cd^{2+} or 5 mM Co^{2+} yielded no inward Ba^{2+} current (data not shown). Although the sustained current in the soma of the *Hermissenda* photoreceptors contained several features that are consistent with L-type Ca^{2+} channels in neurons (Tsien et al., 1988), the single-channel conductance is quite distinct. Typically, the single-channel conductance of L-type Ba^{2+} currents using 70–110 mM as the charge carrier is ~20–30 pS (Fox et al., 1987; Elmslie, 1997; Rodriguez-Contreras and Yamoah, 2001). Single-channel data of L-type channels from rat cerebellar neurons reveal distinct gating patterns at different states, one of which has a different conductance (Forti and Pietrobon, 1993). Thus, the distinct conductance of the BayK 8644-sensitive channels in the photoreceptors may reflect subtle differences between L-type channels, suggestive of different channel subtypes in the L-channel class.

In contrast to the soma, the axons of type B photoreceptors expressed only the sustained current with dihydropyridine sensitivity and activation voltage that is more positive than the 17 pS current (Fig. 2*A*). The single-channel conductance of the axonal Ba^{2+} currents was ~9 pS (Fig. 2*B*). Because similar methods were used to isolate the soma and axons, it is unlikely that the enzyme dissociation procedure used contributed toward the observed differences in channel expression. We determined the kinetics of the axonal Ba^{2+} currents from patches containing single channels to assess their open and shut (closed) times. Figure 3*A* shows the dwell and shut time histograms of the channel at a test potential of 10 mV. The open and shut time

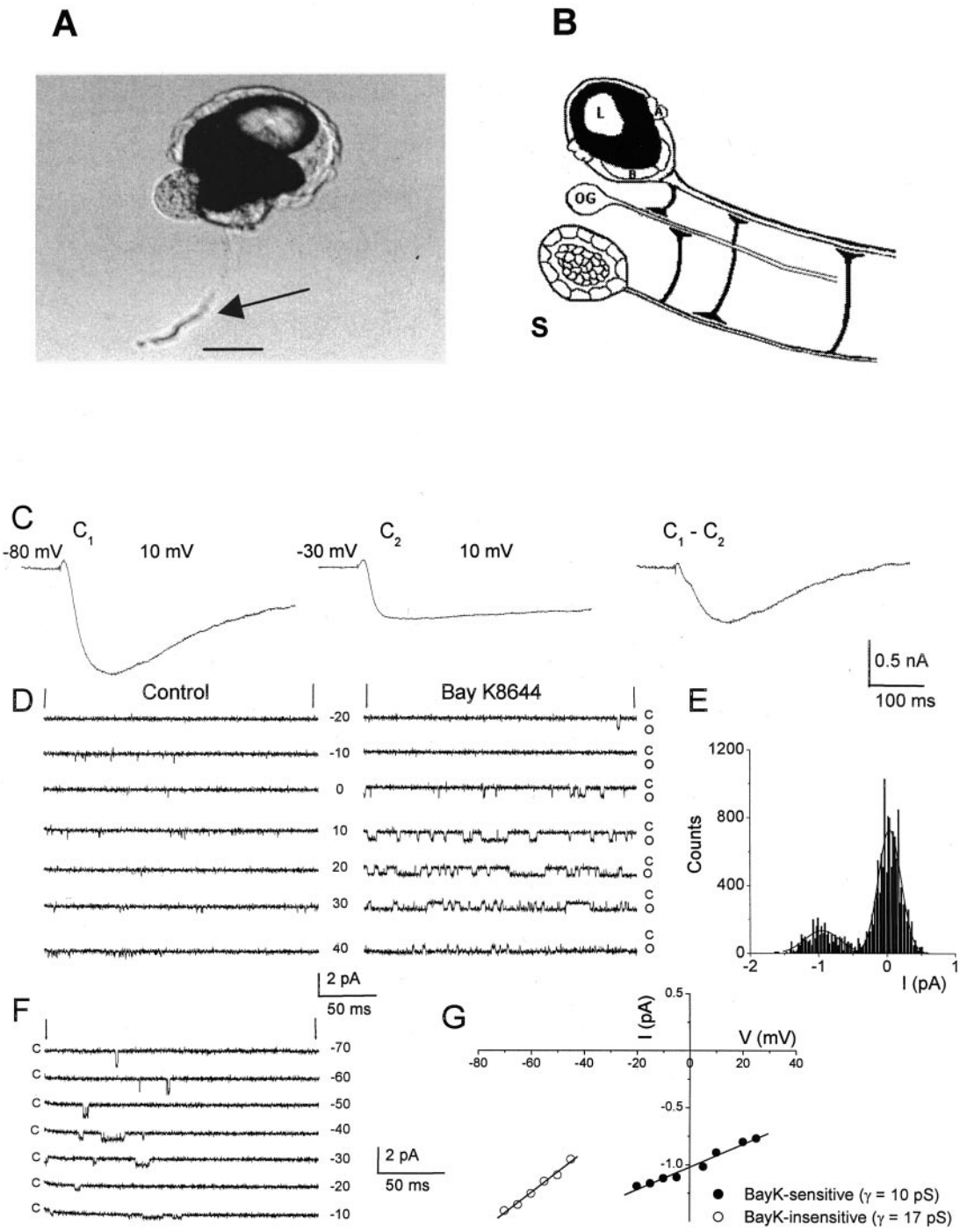

Figure 1. Ca^{2+} currents in soma of type B photoreceptors. *A*, Photomicrograph of isolated *Hermissenda* eye preparation with an intact axon. The *arrow* shows an axon ~120 μm in length. *B*, Schematic diagram of the eye and the statocyst (*S*) with associated synaptic connections along the axons of the photoreceptors. Scale bar, 40 μm. *L*, Lens; *A*, *B*, type B and A photoreceptors; *OG*, optic ganglion. *C*, Whole-cell Ca^{2+} currents recorded by eliminating inward Na^+ currents and suppressing outward K^+ currents with choline substitution of external Na^+ and using bath TEA and 4-AP, respectively. The current trace recorded from a holding potential of −80 mV and a step potential of 10 mV (C_1) consists of a transient and sustained component. The transient component was suppressed when the cell was held at −30 mV (C_2). The difference current ($C_1 - C_2$) revealed the transient current. *D*, A family of seven consecutive sweeps of single-channel current traces recorded in the cell-attached configuration showing brief single-channel opening events. The charge carrier for the single-channel recordings was 250 mM Ba^{2+}. Bath application of 10 μM BayK 8644 resulted in long-duration openings. The holding potential of the patch was −30 mV, and the step potentials are indicated. The closed and open levels are denoted as *C* and *O*, respectively. *E*, Typical amplitude histogram used to determine the unitary amplitude of single-channel currents. The example shown was generated from current traces elicited at a step potential of 20 mV. *F*, In contrast to the BayK 8644-sensitive current, another single-channel current was recorded from the B-cell somata that showed openings at the first 100 msec of the test pulse. The patch pipette contained 20 μM nitrendipine. The current became apparent when patches were held at more negative potentials; the holding potential of the current traces shown is −90 mV, and the step potentials are indicated *beside* the traces. The low voltage-activated current was insensitive to BayK 8644 (data not shown). *G*, The corresponding current–voltage relationships for the BayK 8644-sensitive (●) and -insensitive (○) currents are shown, and the conductances (γ) were 10 and 17 pS, respectively. Analysis of seven patches of BayK 8644-sensitive and -insensitive currents produced a mean conductance (9.7 ± 1.4 pS and 16.6 ± 3.1 pS), respectively.

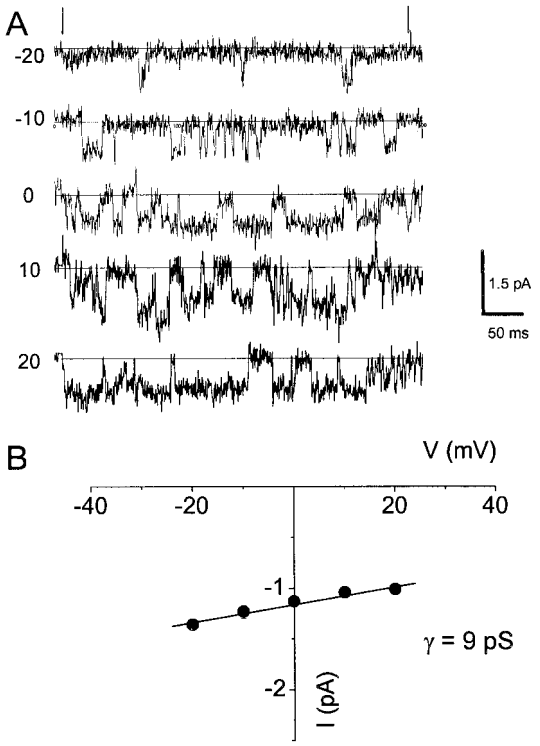

Figure 2. Single-channel Ba^{2+} currents from type B photoreceptor axons. *A*, Representative unitary Ba^{2+} current traces recorded from the photoreceptor axon in the presence of 10 μM BayK 8644 and elicited from a holding potential of −70 mV using test potentials as indicated (*vertical lines* indicate the beginning of the test pulses). *Horizontal lines* represent zero current levels. *B*, The corresponding current–voltage relationship was plotted as mean ± SD. The calculated single-channel conductance (γ) is 9 pS. Summary data from nine similar patches yielded a mean conductance of 8.9 ± 1.5 pS.

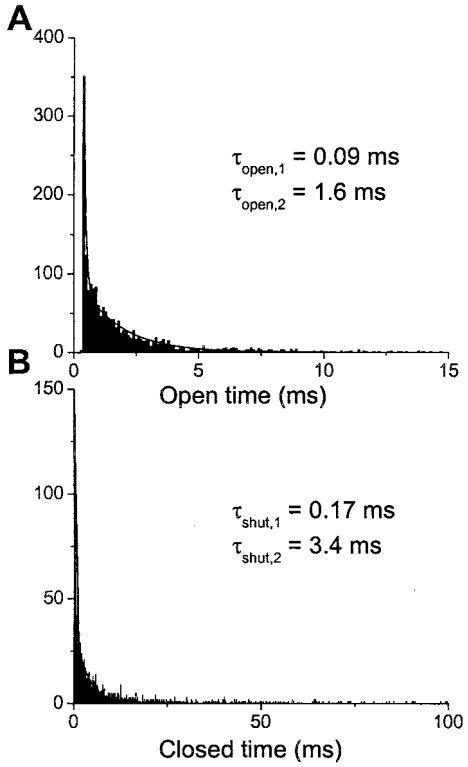

Figure 3. Kinetics of single-channel Ba^{2+} currents in type B photoreceptor axons. *A*, An open-time histogram of axonal single Ba^{2+} currents was generated from traces elicited at a test potential of 10 mV. The histogram was fitted using two exponential functions. The time constants (τ) of the open time for the example shown are indicated. *B*, The shut (closed-time) distribution histogram was also fitted with two τ values as shown. Analyses of the open- and closed-time distribution were performed on axonal patches that contained single channels. Mean data from five patches for the open and shut times of traces elicited at a test potential of 10 mV were as follows: $\tau_{open,1}$ = 0.1 ± 0.06 msec; $\tau_{open,2}$ = 1.8 ± 0.5 msec; $\tau_{shut,1}$ = 0.15 ± 0.08 msec; $\tau_{shut,2}$ = 3.2 ± 1.8 msec.

distributions were best fitted by the sum of two exponential functions, with time constants of open and shut distributions as follows: $\tau_{dwell,1}$ = 0.09 msec and $\tau_{dwell,2}$ = 1.6 msec; $\tau_{shut,1}$ = 0.17 msec and $\tau_{shut,2}$ = 3.4 msec, respectively (Fig. 3*A,B*).

DISCUSSION

Indirect evidence for the differential distribution of Ca^{2+} channels in the somata and axons of neurons has been inferred from action potential-evoked responses from crayfish, lamprey, rat hippocampal, and cerebellar cultured neurons (Delaney et al., 1991; Backsai et al., 1995; Mackenzie et al., 1996; Forti et al., 2000). Moreover, reports using antibodies raised against the Ca^{2+} channel subtypes $Ca_v2.1$, $Ca_v2.2$, and $Ca_v2.3$ have revealed immunohistochemical evidence for the heterogeneous distribution of these Ca^{2+} channels in the axon, dendrites, and soma of neurons (Volsen et al., 1995; Westenbroek et al., 1995). Aside from the important role of voltage-gated Ca^{2+} channels (VGCCs) in mediating Ca^{2+} influx, which is necessary for normal neuronal functions (e.g., triggering of neurotransmitter release), the axonal Ca^{2+} currents may regulate the firing rate of propagated action potentials through activation of Ca^{2+}-dependent K^+ channels (Callewaert et al., 1996). Furthermore, Ca^{2+} storage organelles have been located in axons, raising the possibility that biological phenomena such as Ca^{2+}-induced Ca^{2+} release may occur during the conduction of action potentials and neurotransmitter release (Ogden et al., 1993; Forti et al., 2000). For the type B photoreceptors, differential expression of Ca^{2+} channels may support the compartmentalization of Ca^{2+}-dependent mechanisms, which has been debated as one of the necessary events that may occur during classical conditioning (Crow, 1985; Alkon and Rasmussen, 1988). Typically, Ca^{2+} channels at presynaptic terminals consist of non L-type channels (Wu et al., 1999). However, for synapses in which there is tonic transmitter release, the L-type channel plays a major role in triggering transmitter release, raising the possibility that axonal Ca^{2+} channels in B photoreceptors may mediate tonic release.

The presence of Ca^{2+} microdomains, moreover, may extend beyond axon–soma compartments. There were remarkable variations in the number of channels in axon-attached and null-channel patches, using patch electrodes with similar diameters and resistances. We divided 90 μm axons into proximal, middle, and distal thirds and determined the channel densities of the patches. A total of 59 patches were examined: 16 patches from the proximal third, 19 from the middle third, and 24 from the distal third. Only one patch from the proximal third contained a channel (6%). In addition, the seven patches (37%) in the middle third contained channels, and 22 patches (92%) in the distal third had single-channel or multichannel events. Shown in Figure 4*A* are a family of consecutive current traces recorded from a patch from the distal third of a type B photoreceptor axon. Using the bino-

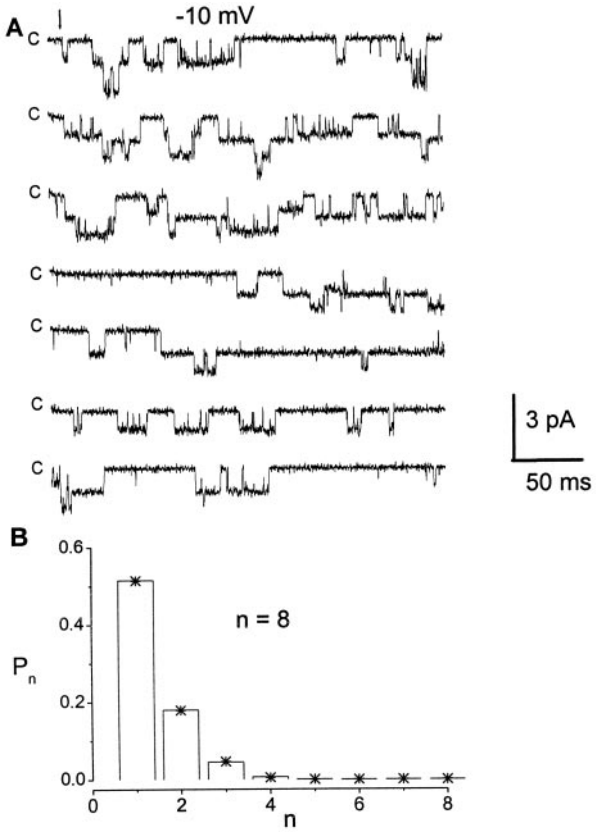

Figure 4. Multiple-channel patches in the distal one-third of a type B photoreceptor axon. *A*, A family of seven consecutive traces recorded from an axon-attached patch at the distal one-third of an ~100 μm axon. The patch was held at −60 mV and stepped to a test potential of −10 mV. The closed levels are indicated as *C*, and the *arrow* denotes the time when the test pulse was initiated. *B*, Bar graphs showing the probability that a given number of channels was open (P_n) against the number of channels (n) obtained from the same patch as *A*. The *columns* represent the experimental data using the measured values for each unitary current level. *Asterisks* indicate the probability (P_n) predicted by the following binomial theorem: $P_n = [N!/n!(N-n)!]P_o^n (1-P_o)^{N-n}$, $n = 0,1,\ldots N$, where N and P_o represent the number of functional channels and the open probability of individual channels, respectively. The predicted probability that an individual channel is open (P_o) = 0.102; the number of functional channels (N) = 8. The capacitance of the patch was estimated to be ~10 pF, and assuming a specific membrane capacitance of 10 mF m^{-2}, the channel density was ~13 channels μm^{-2}. The mean channel density of multiple-channel patches recorded from the distal one-third of the B photoreceptors was 12.7 ± 2.9 channels μm^{-2} (n = 9).

mial distribution, we estimated that there were ~8 channels in the patch (Fig. 4*B*). The capacitance of the patch membrane was estimated to be ~10 pF (Rodriguez-Contreras and Yamoah, 2001). Thus, assuming a specific membrane capacitance of 10 mF m^{-2}, the channel density was determined as N per patch capacitance and expressed as the number of channels per square micrometer.

The axons of the type B photoreceptors serve not only as postsynaptic sites for neuritic projections from the presynaptic hair cells (Alkon and Fuortes, 1972) but also represent presynaptic loci for downstream interneurons (Hodgson and Crow, 1992). Although the present experiments do not allow for identification of the exact synaptic site, *versa vi*, presynaptic and postsynaptic, it would be reasonable to infer that the sites of high Ca^{2+} channel density correspond to the presynaptic regions. The values obtained for the channel density (10–15 channels m^{-2}) resemble the Ca^{2+} channel density in presynaptic terminals of the chick ciliary ganglion and bullfrog saccular hair cells (Haydon et al., 1994; Rodriguez-Contreras and Yamoah, 2001). However, it is equally possible that some of the Ca^{2+} channel clusters and solitary channels may be poised at postsynaptic sites to augment Ca^{2+} influx after neurotransmitter-mediated depolarization.

Axons and dendrites may be involved not only in signal transmission but also in signal transduction. Several forms of neuronal plasticity may be mediated through Ca^{2+} entry into mammalian axons via VGCCs (Callewaert et al., 1996; Beck et al., 2001; Jackson et al., 2001; Verbny et al., 2002). Although Ca^{2+} influx and synaptic contacts between *Hermissenda* hair cells, interneurons, and photoreceptors are crucial to plasticity during conditioning, the exact mechanism remains unknown. Direct measurements of the Ca^{2+} currents in the photoreceptor axons, as described in this study, are a first step toward our understanding of the contribution of axons in the mechanisms underlying conditioning-associated plasticity in *Hermissenda*.

REFERENCES

Alkon DL, Fuortes MG (1972) Responses of photoreceptors in *Hermissenda*. J Gen Physiol 60:631–649.

Alkon DL, Rasmussen H (1988) A spatial-temporal model of cell activation. Science 239:998–1005.

Alkon DL, Lederhendler I, Shoukimas JJ (1982) Primary changes of membrane currents during retention of associative learning. Science 215:693–695.

Alkon DL, Sakakibara M, Forman R, Harrigan J, Lederhendler I, Farley J (1985) Reduction of two voltage-dependent K^+ currents mediates retention of a learned association. Behav Neural Biol 44:278–300.

Alkon DL, Nelson TJ, Zhao W, Cavallaro S (1998) Time domains of neuronal Ca^{2+} signaling and associative memory: steps through a calexcitin, ryanodine receptor, K^+ channel cascade. Trends Neurosci 21:529–537.

Backsai BJ, Wallen P, Lev-Ram V, Grillner S, Tsien RY (1995) Activity-related calcium dynamics in lamprey neurons as revealed by video-rate confocal microscopy. Neuron 14:19–28.

Beck A, Lohr C, Deitmer JW (2001) Calcium transients in subcompartments of the leech Retzius neuron as induced by single action potentials. J Neurobiol 1–18.

Callewaert G, Eilers J, Konnerth A (1996) Axonal calcium entry during fast "sodium" action potentials in rat cerebellar Purkinje neurones. J Physiol (Lond) 495:641–647.

Crow T (1985) Conditioned modification of phototactic behavior in *Hermissenda*. II. Differential adaptation of B-photoreceptors. J Neurosci 5:215–223.

Crow T, Alkon DL (1980) Associative behavioral modification in *Hermissenda*: cellular correlates. Science 209:412–414.

Crow T, Tian LM (2000) Monosynaptic connections between identified A and B photoreceptors and interneurons in *Hermissenda*: evidence for labeled-lines. J Neurophysiol 84:367–375.

Crow T, Tian LM (2002) Morphological characteristics and central projections of two types of interneurons in the visual pathway of *Hermissenda*. J Neurophysiol 87:322–332.

Delaney K, Tank D, Zuker RS (1991) Presynaptic calcium and serotonin-mediated enhancement of transmitter release at crayfish neuromuscular junction. J Neurosci 11:2631–2643.

Elmslie KS (1997) Identification of the single channels that underlie the N-type and L-type calcium currents in bullfrog sympathetic neurons. J Neurosci 17:2658–2668.

Forti L, Pietrobon D (1993) Functional diversity of L-type calcium channels in rat cerebellar neurons. Neuron 10:437–450.

Forti L, Pouzat C, Llano I (2000) Action potential-evoked Ca^{2+} signals and calcium channels in axons of developing rat cerebellar interneurons. J Physiol (Lond) 527:33–48.

Fox AP, Nowycky MC, Tsien RW (1987) Kinetic and pharmacological properties distinguishing three types of calcium currents in chick sensory neurons. J Physiol (Lond) 394:149–172.

Frysztak RJ, Crow T (1997) Synaptic enhancement and enhanced excitability in presynaptic and postsynaptic neurons in the conditioned stimulus pathway of *Hermissenda*. J Neurosci 17:4426–4433.

Hamill OP, Marty A, Neher E, Sakmann B, Sigworth FJ (1981) Improved patch-clamp techniques for high-resolution current recording from cells and cell-free membrane patches. Pflügers Arch 391:85–100.

Haydon PG, Henderson E, Stanley EF (1994) Localization of individual

calcium channels at the release face of a presynaptic nerve terminal. Neuron 13:1275–1280.
Hodgson TM, Crow T (1992) Cellular correlates of classical conditioning in identified light responsive pedal neurons of *Hermissenda crassicornis*. Brain Res 570:267–271.
Jackson VM, Trout SJ, Brain KL, Cunnane TC (2001) Characterization of action potential-evoked calcium transients in mouse postganglionic sympathetic axon bundles. J Physiol (Lond) 537:3–16.
Linden DJ, Ahn S (1999) Activation of presynaptic cAMP-dependent protein kinase is required for induction of cerebellar long-term facilitation. J Neurosci 19:10221–10227.
Lynch G, Kessler M, Arai A, Larson J (1990) The nature and causes of hippocampal long-term facilitation. Prog Brain Res 436:177–183.
Mackenzie PJ, Umemiya M, Murphy TH (1996) Ca^{2+} imaging of CNS axons in culture indicates reliable coupling between single action potentials and distal functional release sites. Neuron 16:783–795.
Malenka RC, Nicoll RA (1999) Long-term potentiation–a decade of progress? Science 285:1870–1874.
Ogden DC, Khodakhah K, Carter TD, Gray PT, Capiod T (1993) Mechanisms of intracellular calcium release during hormone and neurotransmitter action investigated with flash photolysis. J Exp Biol 184:105–127.
Rodriguez-Contreras A, Yamoah EN (2001) Direct measurement of single-channel Ca^{2+} currents in bullfrog hair cells reveals two distinct channel subtypes. J Physiol (Lond) 534:669–689.
Schuman EM, Clark GA (1994) Synaptic facilitation at connections of *Hermissenda* type B photoreceptors. J Neurosci 14:1613–1622.
Staubli U, Rogers G (1994) Facilitation of glutamate receptors enhances memory. Proc Natl Acad Sci USA 91:777–781.
Tomsic D, Alkon DL (2000) Background illumination effects upon *in vitro* conditioning in *Hermissenda*. Neurobiol Learn Mem 74:56–64.
Tsien RW, Lipscombe D, Madison DV, Bley KR, Fox AR (1988) Multiple types of neuronal calcium channels and their selective modulation. Trends Neurosci 11:431–438.
Verbny Y, Zhang C-L, Chiu SY (2002) Coupling of calcium homeostasis to axonal sodium in axons of mouse optic nerve. J Neurophysiol 88:802–816.
Volsen SG, Day NC, McCormack AL, Smith W, Craig PJ, Beattie R, Ince PG, Shaw PJ, Ellis SB, Gillespie A, Harpold MM, Lodge D (1995) The expression of neuronal voltage-dependent calcium channels in human cerebellum. Brain Res Mol Brain Res 34:271–282.
Westenbroek RE, Sakurai T, Elliott EM, Hell JW, Starr TV, Snutch TP, Catterall WA (1995) Immunochemical identification and subcellular distribution of the α1A subunits of brain calcium channels. J Neurosci 15:6403–6418.
Wu L-G, Westenbroek RE, Borst JGG, Catterall WA, Sakmann B (1999) Calcium channel types with distinct presynaptic localization couple differentially to transmitter release in single calyx-type synapses. J Neurosci 19:726–736.
Yamoah EN, Crow T (1994) Two components of calcium currents in the soma of photoreceptors of *Hermissenda*. J Neurophysiol 72:1327–1336.
Yamoah EN, Crow T (1996) Protein kinase and G-protein regulation of Ca^{2+} currents in *Hermissenda* photoreceptors by 5-HT and GABA. J Neurosci 16:4799–4809.
Yamoah EN, Kuzirian AM, Sanchez-Andres JV (1994) Calcium current and inactivation in identified neurons in *Hermissenda*. J Neurophysiol 72:2198–2207.
Yamoah EN, Matzel L, Crow T (1998) Expression of different types of inward rectifier currents confers specificity of light and dark responses in type A and B photoreceptors of *Hermissenda*. J Neurosci 18:6501–6511.